Rapid Communications

Robust emergence of a topological Hall effect in MnGa/heavy metal bilayers

K. K. Meng,[1,*] X. P. Zhao,[2] P. F. Liu,[1] Q. Liu,[1] Y. Wu,[1] Z. P. Li,[1] J. K. Chen,[1] J. Miao,[1] X. G. Xu,[1] J. H. Zhao,[2] and Y. Jiang[1,†]

[1]*School of Materials Science and Engineering, University of Science and Technology Beijing, Beijing 100083, China*

[2]*State Key Laboratory of Superlattices and Microstructures, Institute of Semiconductors, Chinese Academy of Sciences, Beijing 100083, China*

(Received 15 November 2017; revised manuscript received 12 February 2018; published 22 February 2018)

We have investigated the topological Hall effect (THE) in MnGa/Pt and MnGa/Ta bilayers induced by the interfacial Dzyaloshinskii-Moriya interaction (DMI). By varying the growth parameters, we can modulate the domain wall energy, and the largest THE signals are found when the domain wall energy is the smallest. The large topological portion of the Hall signal from the total Hall signal has been extracted in the whole temperature range from 5 to 300 K. These results open up the exploration of the DMI induced magnetic behavior based on the bulk perpendicular magnetic anisotropy materials for fundamental physics and magnetic storage technologies.

DOI: 10.1103/PhysRevB.97.060407

The exchange interactions allow the magnetic moments in a solid to communicate with each other and lie at the heart of the phenomenon of long-range magnetic order [1]. In the early days of quantum mechanics, the Heisenberg exchange interaction was recognized to determine the types of magnetic ground state. It can be shown as a relatively simple form $J_{12}\mathbf{S_1}\cdot\mathbf{S_2}$, where J_{12} is the exchange constant; $\mathbf{S_1}$ and $\mathbf{S_2}$ are the total spin of two nearby atoms. The sign of J_{12} (positive or negative) determines the coupling modes of $\mathbf{S_1}$ and $\mathbf{S_2}$ (ferromagnetic or antiferromagnetic). However, the spin-orbit coupling (SOC) will also exert influence on the exchange interactions. On one hand, it connects the magnetization direction to the crystal lattice, and the resulting variation of magnetic energy is referred to as magnetic anisotropy. On the other hand, in the magnetic systems that lack inversion symmetry (whether due to underlying crystal structure or interfaces), SOC can combine with the exchange interaction to generate an anisotropic exchange interaction that favors a chiral arrangement of the magnetization [2,3]. This is known as the Dzyaloshinskii-Moriya interaction (DMI), which has a form $\mathbf{D}_{12}\cdot(\mathbf{S_1}\times\mathbf{S_2})$. The vector $\mathbf{D}_{12}$ depends on the details of electron wave functions and could point to different directions, which depends on the symmetry and the precise crystalline structure. Contrary to the Heisenberg exchange interaction, which leads to collinear alignment of lattice spins, this form of DMI therefore very often cants the spins by a small angle. If the DMI is strong enough to compete with the Heisenberg exchange interaction and the magnetic anisotropy, it can stabilize chiral domain wall structures such as the skyrmion. When a conduction electron passes through a chiral domain wall, the spin of the conduction electron will experience a fictitious magnetic field (Berry curvature) in real space, which deflects the conduction electrons perpendicular to the current direction [4,5]. Therefore, it will cause an additional contribution to the observed Hall signals that has been termed the topological Hall effect (THE) [4,5]. THE can be described by the same theoretical scheme as the intrinsic anomalous Hall effect (AHE), which has been clarified to be a Berry phase in momentum space [6].

The recently reported THE in the bulk noncentrosymmetric crystalline structure in B20-type magnets has demonstrated its promise as a tool for probing DMI [7,8]. Besides the bulk-type DMI, recent extensive experiments have been focused on the interfacial-type DMI in heavy metal/ferromagnet (HM/FM) bi- and multilayers due to the inherent tunability of magnetic interactions in two dimensions [9–15]. In ultrathin films which are thinner than the domain wall width and DMI associated length, the domain wall energy with interfacial DMI can be written as $\sigma = 4\sqrt{AK} - \pi D$, where D is the effective DMI energy constant, A the exchange constant, and K the anisotropy constant [16,17]. For the most favorable chirality, it lowers the energy. The limit of this situation is when σ goes to zero, which defines the critical DMI energy constant $D_c = 4\sqrt{AK}/\pi$. Therefore, the domain wall energy would be negative and the chiral domain walls should proliferate if $D > D_c$, and the methods that can modulate D and D_c to decrease σ have been explored. To induce a much larger DMI at the interfaces, Moreau-Luchaire *et al.* have designed the Co-based multilayered thin films in which the Co layer is sandwiched between Ir and Pt layers, which will lead to additive interfacial chiral interactions that increase the effective DMI of the magnetic layer since the two HMs induce interfacial chiral interactions of opposite symmetries and parallel $\mathbf{D}_{12}$ [9]. By harnessing the large and opposite signs of DMI generated from Fe/Ir and Co/Pt interfaces, Soumyanarayanan *et al.* achieved substantial control over the effective DMI governing skyrmion properties in the Ir/Fe/Co/Pt multilayers [12]. The inclusion of Fe results in the gradual formation of a Fe/Ir interface and corresponding suppression of the Co/Ir boundary, leading to increasing DMI and evident THE. More importantly, by varying the ferromagnetic layer composition and thickness, they can modulate D_c. When $D > D_c$, the skyrmions become thermodynamically stable entities, which is particularly important for technological applications.

In this work, we present the large THE in MnGa/Pt and MnGa/Ta bilayers, in which the MnGa layer exhibits bulk

*kkmeng@ustb.edu.cn
†yjiang@ustb.edu.cn

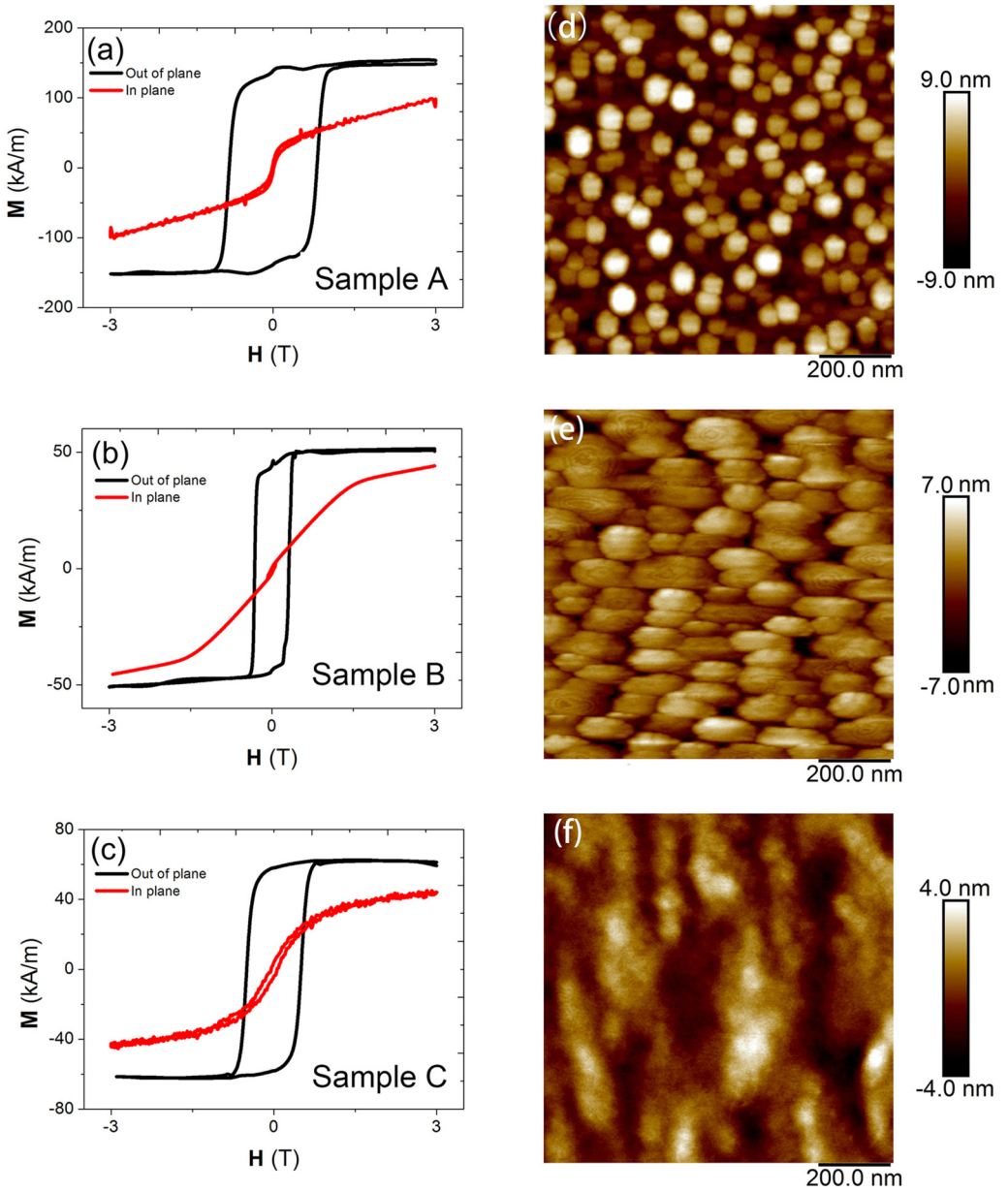

FIG. 1. (a–c) Hysteresis loops for the out-of-plane and in-plane magnetizations of the three samples at 300 K. (d–f) AFM images of samples A–C (scale bar, 200 nm).

perpendicular magnetic anisotropy (PMA). The value of D is considered to be constant with the same HM capping layer. Therefore, by varying the growth parameters of MnGa, we can modulate D_c to decrease σ, and the largest THE signals are found when σ is the smallest. We clearly demonstrate the extraction of the large topological portion of the Hall signal from the total Hall signal in the whole temperature range from 5 to 300 K and determine the magnitude of the fictitious magnetic field.

The nominal 1-nm-thick MnGa films were firstly grown on 100-nm-thick GaAs buffered semi-insulating GaAs (001) substrates by molecular-beam epitaxy. The growth temperatures have been set at 80 °C, 60 °C, and 40 °C for three samples denoted as samples A, B, and C, respectively. Then the samples were annealed at 300 °C for 1 min. Finally, other nominal 3-nm-thick MnGa films were continued to be grown at 300 °C after the annealing. The thickness of the MnGa films has been controlled by the flux of Mn and Ga atoms referred to in our previous works [18,19]. Figures 1(a)–1(c) show both the out-of-plane and in-plane hysteresis loops of the three samples. The strong difference between the out-of-plane and in-plane curves

TABLE I. Saturation magnetization M_s, the anisotropy field H_k, uniaxial PMA constant K, the critical DMI energy constant D_c, and the root-mean square roughness R_q of the three samples.

Sample	M_s(kAm^{-1})	H_k (T)	K (kJ/m^3)	D_c(mJ/m^2)	R_q (nm)
A	145	13.7	993	1.82	3.6
B	51	4.5	115	0.652	2.6
C	63	9.5	299	1.08	1.1

reveals giant bulk PMA in these films. From the magnetization measurements we can get the following parameters: saturation magnetization M_s, the anisotropy field H_k, and uniaxial PMA constant $K = M_s H_k/2$. The exchange constant $A(\sim 2.3\,\mathrm{pJ/m})$ is considered to be the same for the three samples [20]. Finally, the D_c can be determined and all the parameters have been summarized in Table I. Therefore, we will focus on the performance of the magnetic and transport properties based on sample B, in which the smallest D_c results in the smallest σ. Figures. 1(d)–1(f) show atomic force microscopy (AFM) images for three samples. It is found that the grains with the size ranging from 30 to 300 nm have been formed

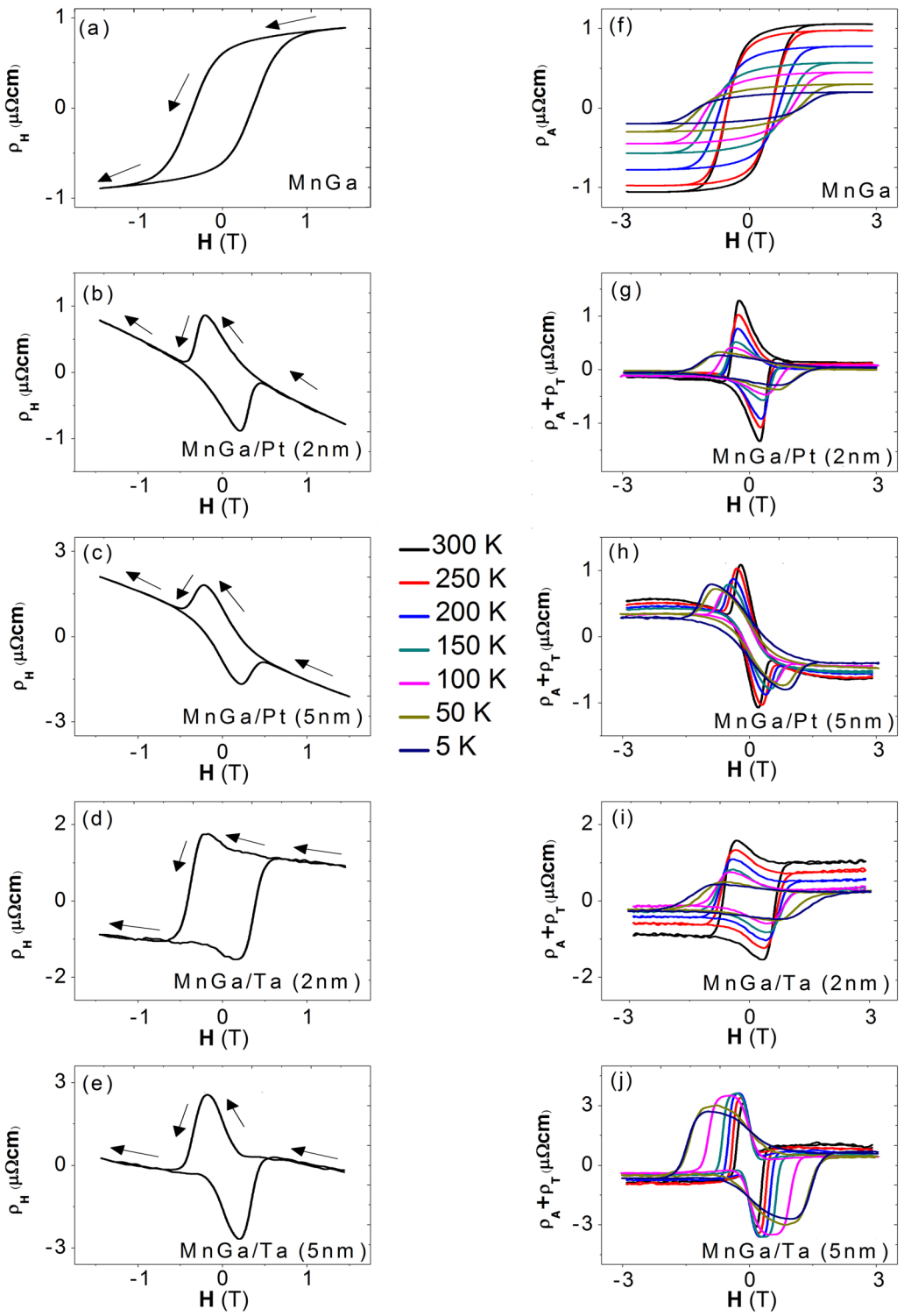

FIG. 2. (a–e) Total Hall resistivities in the single MnGa, MnGa/Pt (t), and MnGa/Ta (t) ($t = 2{,}5$ nm) films at 300 K. The arrows denote the change tendency of Hall resistivity when the magnetic field is applied from positive to negative. (f–j) ($\rho_A + \rho_T$) vs H for the single MnGa, MnGa/Pt (t), and MnGa/Ta (t) ($t = 2{,}5$ nm) films in the temperature range from 5 to 300 K.

in the samples A, B, and C. The surface root-mean square roughness R_q of the three samples has also been summarized in Table I. Although the R_q of sample B is relatively large, the grains shared the same orientation as proved by the x-ray diffraction (XRD) measurements as shown in Fig. S1 of the Supplemental Material [21]. Finally, sample B was transferred to the magnetron sputtering system immediately through a lower vacuum chamber, which is similar to our previous works [18,19], and the films revealed good interface properties and eliminated other interface effects. The Pt and Ta layers with different thicknesses were then deposited and a 2-nm-thick Al film was also deposited on sample B to prevent oxidation, but we denote sample B/Al (2 nm) bilayers as a single MnGa film in this Rapid Communication. Photolithography and Ar ion milling are used to pattern Hall bars and the lift-off process is used to form the contact electrodes. The size of all the Hall bars is 10 μm $\times$ 80 μm (Supplemental Material [21]), which is the same as in our previous work [19]. To determine the DMI at the MnGa/HMs interfaces, we looked into the field dependence of the Hall resistivities in MnGa/Pt (t) and MnGa/Ta (t) (t = 2 and 5 nm) bilayers in the whole temperature range from 5 to 300 K, which are compared with the results in a single MnGa film. Considering the different thickness of MnGa and HM films, the anomalous Hall resistivity, the topological Hall resistivity, and the longitudinal resistivity in this Rapid Communication have been defined with respect to those of the MnGa layer with the assumption that each film acts as a parallel resistance path [19]. We have measured the temperature-dependent resistivities of single Al, Pt, and Ta films, and the definition of the resistivity in MnGa layer has been shown in Ref. [21]. The results are shown in Figs. 2(a)–2(e), where it is found that the deposited Pt and Ta layers have given rise to anomalies in the Hall resistivities, which show a bump or dip during the hysteretic measurements. The total Hall resistivity can usually be expressed as the sum of various contributions [8]:

$$\rho_H = R_0 \mathrm{H} + \rho_\mathrm{A} + \rho_\mathrm{T}, \tag{1}$$

where R_0 is the normal Hall coefficient, ρ_A the anomalous Hall resistivity, and ρ_T the topological Hall resistivity.

In Figs. 2(a)–2(e), the THE signals clearly coexist with the large background of normal Hall effect and AHE. To more clearly demonstrate it, we have subtracted the normal Hall term and the temperature dependence of $(\rho_\mathrm{A} + \rho_\mathrm{T})$ have been shown in Figs. 2(f)–2(j). After the subtractions, we can further discern the peak and hump structure in the whole temperature range, which can be attributed to the THE term. On the other hand, the interface transport properties should depend on both the MnGa and HM layers, though we have subtracted the contribution from the HM layers [21]. The combination of different polarities of the normal Hall coefficient in MnGa and Pt layers has changed the sign of $(\rho_\mathrm{A} + \rho_\mathrm{T})$ in the MnGa/Pt (5 nm) bilayers as compared with that in other films. The AHE contribution ρ_A can be expressed as [6]

$$\rho_\mathrm{A} = \alpha M \rho_{xx0} + b M \rho_{xx}^2, \tag{2}$$

where ρ_{xx0} is the residual resistivity induced by impurity scattering, ρ_{xx} the longitudinal resistivity, M the magnetization, and α and b the coefficients. The first term is the extrinsic contribution from both the side jump and skew scattering, and the second term is the intrinsic contribution. Therefore, to extract the THE term ρ_T, the magnetoresistance (MR) and magnetization in the whole temperature range should be firstly investigated.

MR is expressed as $\mathrm{MR} = [\rho_{xx}(H) - \rho_{xx}(0)]/\rho_{xx}(0)$ and the results of the single MnGa, MnGa/Pt (5 nm) and MnGa/Ta (5 nm) films have been taken as representatives as shown in Fig. 3. The AMR of single MnGa film shows similar behavior to that our previous work [18]. More interestingly, dip structures in the AMR curves have been found in the MnGa/Pt (5 nm) and MnGa/Ta (5 nm) bilayers around zero magnetic field. It indicates that the electrons experience a more complicated electromagnetic field due to the presence of nonzero Berry curvature in real space, which becomes stable and plays a more significant role in the transport properties when the applied magnetic field is smaller than the coercivity. Note that the origin of MR is connected with SOC and its influence on *s-d* scattering, and the orbital magnetic moment and the topology of the Fermi surface will be influenced by the strong SOC of the deposited HM layers. Correspondingly, in

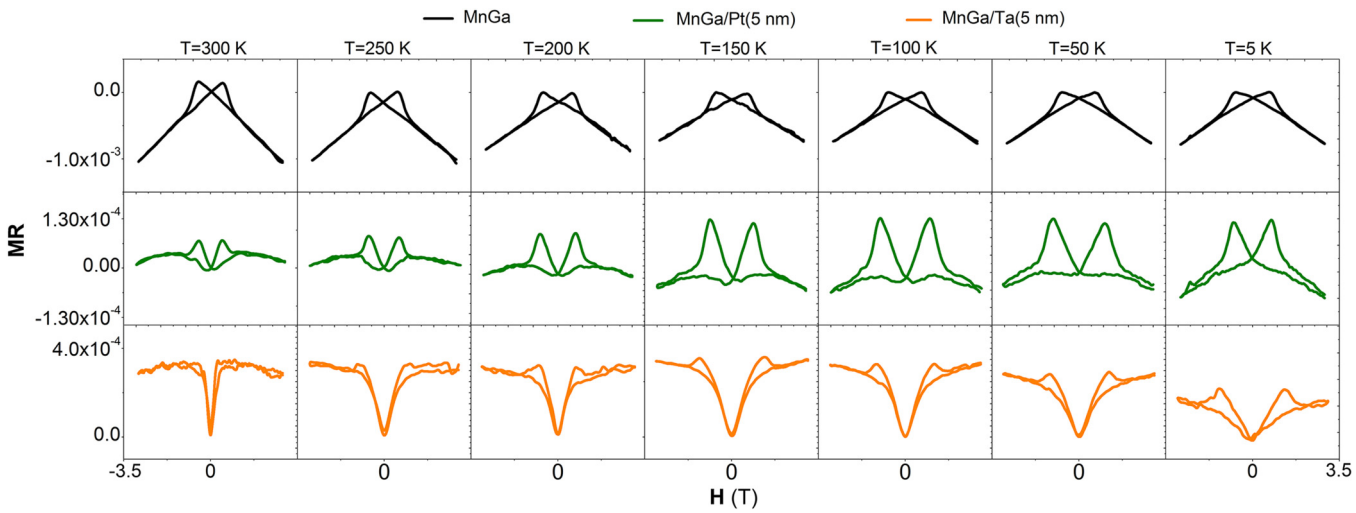

FIG. 3. Magnetoresistance of the single MnGa, MnGa/Pt (5 nm), and MnGa/Ta (5 nm) films in the temperature range from 5 to 300 K.

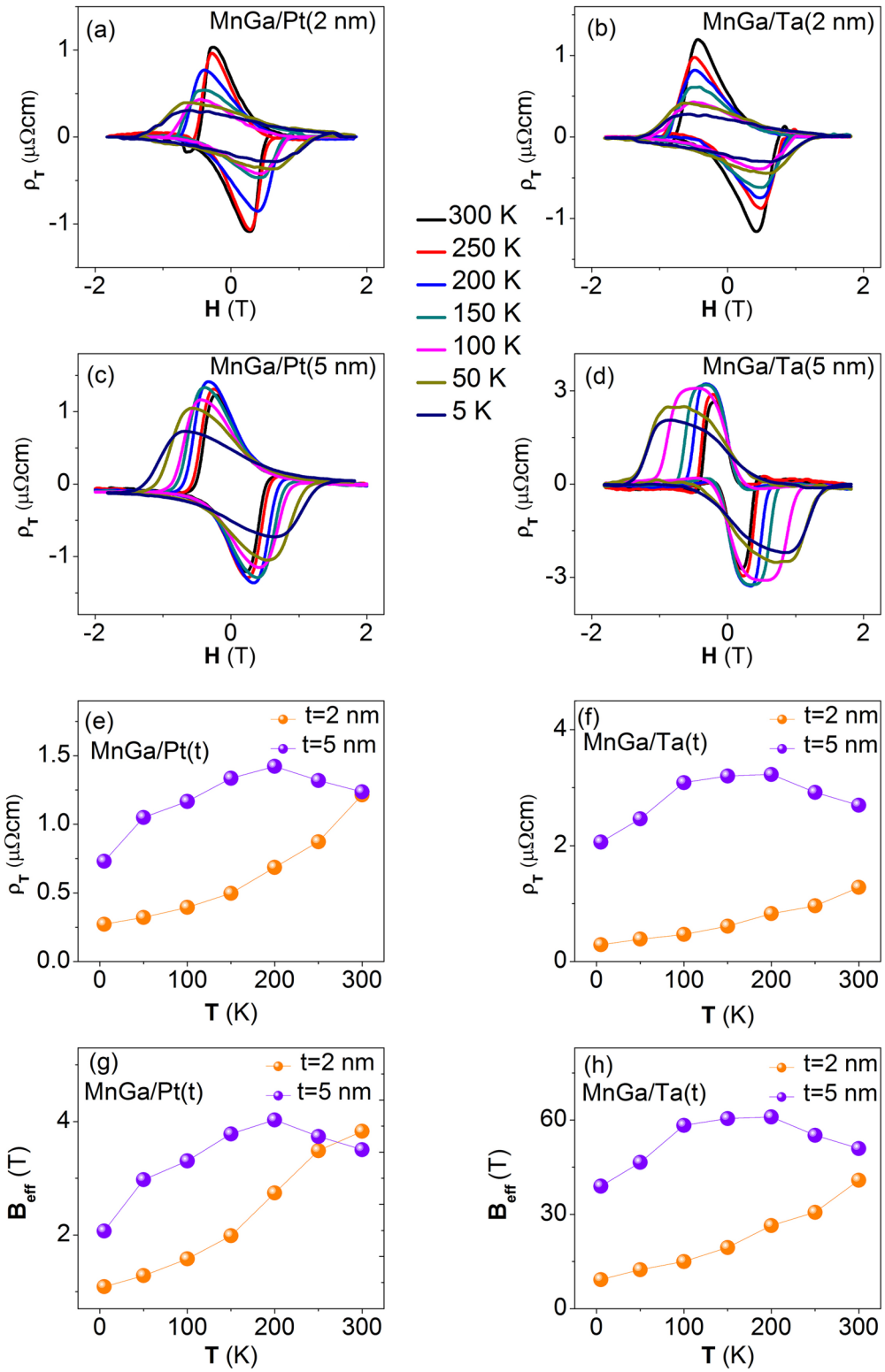

FIG. 4. (a–d) $\rho_T(H)$ in MnGa/Pt(t) and MnGa/Ta(t) ($t = 2,5$ nm) films at different temperatures. (e,f) Temperature dependence of ρ_T for all the films. (g,h) show the temperature dependence of fictitious magnetic field B_{eff} in all the films.

this case, the electron energy will be modified by the orbital magnetic moment and the electron velocity gains an extra velocity term proportional to the Berry curvature in real space [22]. At the high-field limit, i.e., $\omega_c\tau \gg 1$, where ω_c is the cyclotron frequency and τ is the relaxation time, the total current in the crossed electric and magnetic fields is the Hall current, suggesting that even in the presence of AHE, the high-field Hall current gives the "real" electron density. It can explain the larger THE signals appearing between zero field and the coercivities. On the contrary, at the low-field limit, i.e.,

$\omega_c\tau \ll 1$, the Berry phase will induce a linear MR as $\sigma_{xx} \approx \sigma_{xx}^{(0)} + \sigma_{xx}^{(1)}$, where $\sigma_{xx}^{(0)}$ is the zero field conductivity, $\sigma_{xx}^{(1)} \propto B_{\text{eff}}$, and B_{eff} is the fictitious magnetic field. It may explain the nearly linear MR behaviors around the zero magnetic field, which is much more evident in the MnGa/Ta (5 nm) bilayer due to a stronger fictitious magnetic field. On the other hand, the unusual MR can also be ascribed to the field-related magnetic textures which can be visualized in the M-H curves as shown in Fig. S4 [21].

After accounting for the longitudinal resistivity and magnetization, now we can extract the THE term ρ_{T}. As the topological Hall resistivity should vanish when the ferromagnetic magnetic collinear state is induced, the coefficients in Eq. (2) can be determined by describing the AHE resistivity ρ_T in terms of the longitudinal resistivity ρ_{xx} in a high-field region [21]. The extracted ρ_{T} in all the films have been shown in Figs. 4(a)–4(d). It is assumed to be a unique signature of THE, and the temperature dependences of the largest ρ_{T} in all the bilayers have been shown in Figs. 4(e) and 4(f). The THE is evident in the whole temperature range from 5 to 300 K, which is much different from that in B20-type bulk chiral magnets subjected to low temperature and large magnetic field [7,8]. Notably, the difference of the THE signals between 2- and 5-nm Ta capping layers is larger than that in MnGa/Pt (t) films. Clevenger *et al.* have demonstrated that the resistivity of α phase Ta film ($\sim 50\,\mu\Omega\,\text{cm}$) is much lower than its β phase ($\sim 200\,\mu\Omega\,\text{cm}$) [23], which dramatically depends on the deposition conditions and stress relaxation, and the β-Ta has stronger SOC [24]. Although the resistivity of a 2-nm-thick Ta film is very close to that in a 5-nm-thick film as shown in Fig. S3 [21], the phase may be different since the thinner film is more susceptible to interface stress and oxidation. Meanwhile, though the 2-nm-thick Ta should be oxidized to some extent, the SOC and spin Hall angle are considered to be not strongly influenced as discussed in the work of Woo *et al.* [25]. On the other hand, the different coverage on the MnGa grains will also modify the effective SOC. Therefore, the interfacial DMI should be varied by these effects.

Since the fictitious magnetic field acts like the classical magnetic field in the same manner as the normal Hall effect, the measured THE signals can be written as $\rho_{\text{T}} = PR_0B_{\text{eff}} = PR_0n_\phi^{\text{T}}\phi_0$, where P is the spin polarization of charge carriers and determined to be 40% for all the films [26], R_0 denotes the normal Hall coefficient, and B_{eff} the fictitious magnetic field, $\phi_0 = h/e$ is the flux quantum, and n_ϕ^{T} is the chiral domain wall density [12,13]. Then the temperature dependences of B_{eff} in all the films can be deduced and have been summarized in Figs. 4(g) and 4(h). The variation tendency is similar to ρ_{T}, and the largest values at 200 K have been found in both MnGa/Pt (5 nm) and MnGa/Ta (5 nm) bilayers, which depends on the whole set of magnetic parameters and DMI. The B_{eff} values of MnGa/Ta (5 nm) in the whole temperature are all much larger than the bulk-type DMI derived fictitious magnetic field under low temperature and large field [7,8]. At room temperature, the n_ϕ^{T} is calculated to be $\sim 800\,\mu\text{m}^{-2}$ and $\sim 1 \times 10^4\,\mu\text{m}^{-2}$ in MnGa/Pt (5 nm) and MnGa/Ta (5 nm) bilayers, respectively. We can also approximately estimate that the separation of the chiral domain walls $[(n_\phi^{\text{T}})^{-1/2}]$ is ~ 35 nm and ~ 10 nm in these two films, which also indicates the length scale of the skyrmion because its lower limit should be larger than the film thickness of ~ 4 nm due to the two-dimensional nature of the skyrmion. The values are area averaged and can be even smaller due to the coexistence between the skyrmion and the ferromagnetic phase. On the other hand, based on the MnGa films shown in this Rapid Communication, the value of D at the MnGa/Pt interfaces would be around $1.08\,\text{mJ/m}^2$ since a weak THE emerged in sample C/Pt (5 nm) bilayers [21]. According to the magnetic parameters as shown in Table I, the nominal domain wall width $\Delta = \sqrt{A/K}$ of sample B is ~ 4.47 nm and the DMI associated length $\xi = 2A/D$ is considered to be ~ 4.26 nm based on MnGa/Pt bilayers, which are all larger than the nominal thickness ~ 4 nm of sample B. Therefore, the domain wall structures in MnGa/HMs bilayers can be explained by the theory of Thiaville *et al.*, where they have investigated by micromagnetics a new domain wall structure in ultrathin films with perpendicular anisotropy, as a result of the DMI from the adjacent layers [17]. The Néel domain wall structure with a fixed chirality will be finally stabilized when D is larger than D_c, and the domain wall width Δ is considered to be constant during the transition. With the introduction of interfacial DMI to sample B, the domain wall structures in MnGa/Pt and MnGa/Ta bilayers will be Néel type with fixed chirality, and the domain wall widths in both of the films are considered to be similar to that in sample B ($\Delta = 4.47$ nm). Therefore, the size of the chiral domain walls in the sample B/Pt and sample B/Ta bilayers are considered to be the same but the separation is different according to the discussion of $(n_\phi^{\text{T}})^{-1/2}$.

Notably, the SOC plays different roles in Spin Hall effect (SHE) as compared with the interfacial DMI, since there is no obvious connection between the strength and sign of SHE and those of the interfacial chiral DMI. It is suggested by the similar behavior of ρ_{T} in the MnGa/Pt and MnGa/Ta films, though the spin Hall angles in Pt and Ta are opposite in sign. Recently, using relativistic first-principles calculations, Belabbes *et al.* have shown that the chemical trend of the DMI in 3d-5d ultrathin films follows Hund's first rule with a tendency similar to their magnetic moments in either the unsupported 3d monolayers or 3d-5d interfaces [27]. The driving force is the 3d orbital occupations and their spin-flip mixing processes with the spin-orbit active 5d states directly controlling the sign and magnitude of DMI. The largest absolute DMI value is obtained in Mn/5d films, indicating that DMI does depend critically not only on SOC and the lack of the inversion symmetry, but also on the d wave function hybridization of the 3d-5d interface. Therefore, in addition to SOC, the Hund's exchange and crystal-field splitting of d orbitals should also be considered in the origin of DMI. Based on this scenario, to some extent, the large THE in the MnGa/Pt and MnGa/Ta films can be partly ascribed to the degree of hybridization between Mn/Pt and Mn/Ta states around the Fermi level. Mn has five filled 3d orbitals with all spin-up states, where the spin-up (spin-down) channels are totally occupied (unoccupied), so that all the possible transitions between these states will contribute to DMI.

It should be noted that the suitable design of MnGa films will decrease the D_c and σ, making the DMI energy more prominent in the total magnetic energies [28,29]. We have also compared the THE in sample A/Pt (5 nm) and sample C/Pt (5 nm) bilayers and a weak THE only emerged in sample

C/Pt bilayers [21]. In our previous works, we have investigated the spin-orbit torque (SOT) in the MnGa/HMs films [18,19], in which the MnGa layer is continuous film ($R_q = 0.4$ nm) and the D_c is calculated to be $\sim 1.11\,\mathrm{mJ/m^2}$ [21]. However, we have not found THE in these films though the value of D_c is very close to that in sample C as shown in Table I. Therefore, it seems that the grain structures will promote the formation of THE, which needs further investigation. We have also investigated the SOT in MnGa/Pt (5 nm) bilayers based on the three samples. The SOT driven magnetization switching only emerged in the sample C/Pt bilayers [21], and the magnetization has not been fully switched. The SOT driven magnetization switching is supposed to be subdued for grain films, and the domain wall motion will be strongly influenced by the grain sizes though there is THE in both sample B/Pt and sample C/Pt bilayers. Furthermore, in the calculation we have determined the same value of A for the three samples, which actually will change due to the structural disorders of the MnGa films [30]. Based on a simple assumption in the Stoner model for itinerant ferromagnetism, the smaller saturation magnetization in samples B and C can be an index of the weak exchange interaction [31]. Therefore, the role of DMI in SOT driven magnetization switching and THE based on MnGa films should be further exploited.

In summary, we have demonstrated the presence of large THE in the MnGa/Pt and MnGa/Ta bilayers induced by strong interfacial DMI between HMs (Pt and Ta) and Mn atoms. The largest THE signals have been found based on the MnGa films with smallest D_c, which correspondingly results in the smallest σ. The large topological portion of the Hall signal from the total Hall signal has been extracted in the whole temperature range from 5 to 300 K and the magnitude of the fictitious magnetic field has been determined. These results open up the exploration of the DMI induced magnetic behavior based on the bulk PMA materials for fundamental physics and magnetic storage technologies.

This work was partially supported by the National Basic Research Program of China (Grant No. 2015CB921502), the National Science Foundation of China (Grants No. 51731003, No. 61404125, No. 51471029, No. 51671019, No. 11574027, No. 51501007, No. 51602022, No. 61674013, and No. 51602025), and the Fundamental Research Funds for the Central Universities (Grant No. FRF-GF-17-B6).

[1] Y. Taguchi, Y. Oohara, H. Yoshizawa, N. Nagaosa, and Y. Tokura, Science **291**, 2573 (2001).
[2] I. Dzyaloshinsky, J. Phys. Chem. Solids **4**, 241 (1958).
[3] T. Moriya, Phys. Rev. **120**, 91 (1960).
[4] J. Ye, Y. B. Kim, A. J. Millis, B. I. Shraiman, P. Majumdar, and Z. Tešanovic, Phys. Rev. Lett. **83**, 3737 (1999).
[5] P. Bruno, V. K. Dugaev, and M. Taillefumier, Phys. Rev. Lett. **93**, 096806 (2004).
[6] N. Nagaosa, J. Sinova, S. Onoda, A. H. MacDonald, and N. P. Ong, Rev. Mod. Phys. **82**, 1539 (2010).
[7] Y. Li, N. Kanazawa, X. Z. Yu, A. Tsukazaki, M. Kawasaki, M. Ichikawa, X. F. Jin, F. Kagawa, and Y. Tokura, Phys. Rev. Lett. **110**, 117202 (2013).
[8] N. Kanazawa, Y. Onose, T. Arima, D. Okuyama, K. Ohoyama, S. Wakimoto, K. Kakurai, S. Ishiwata, and Y. Tokura, Phys. Rev. Lett. **106**, 156603 (2011).
[9] C. Moreau-Luchaire, C. Moutafis, N. Reyren, J. Sampaio, C. A. F. Vaz, N. Van Horne, K. Bouzehouane, K. Garcia, C. Deranlot, P. Warnicke, P. Wohlhüter, J.-M. George, M. Weigand, J. Raabe, V. Cros, and A. Fert, Nat. Nanotechnol. **11**, 444 (2016).
[10] S. Woo, K. Litzius, B. Krüger, M.-Y. Im, L. Caretta, K. Richter, M. Mann, A. Krone, R. M. Reeve, M. Weigand, P. Agrawal, I. Lemesh, M.-A. Mawass, P. Fischer, M. Kläui, and G. S. D. Beach, Nat. Mater. **15**, 501 (2016).
[11] O. Boulle, J. Vogel, H. Yang, S. Pizzini, D. de Souza Chaves, A. Locatelli, T. Onur Menteş, A. Sala, L. D. Buda-Prejbeanu, O. Klein, M. Belmeguenai, Y. Roussigné, A. Stashkevich, S. M. Chérif, L. Aballe, M. Foerster, M. Chshiev, S. Auffret, I. M. Miron, and G. Gaudin, Nat. Nanotechnol. **11**, 449 (2016).
[12] A. Soumyanarayanan, M. Raju, A. L. G. Oyarce, A. K. C. Tan, M.-Y. Im, A. P. Petrović, P. Ho, K. H. Khoo, M. Tran, C. K. Gan, F. Ernult, and C. Panagopoulos, Nat. Mater. **16**, 898 (2017).
[13] J. Matsuno, N. Ogawa, K. Yasuda, F. Kagawa, W. Koshibae, N. Nagaosa, Y. Tokura, and M. Kawasaki, Sci. Adv. **2**, e1600304 (2016).
[14] M. Bode, M. Heide, K. von Bergmann, P. Ferriani, S. Heinze, G. Bihlmayer, A. Kubetzka, O. Pietzsch, S. Blügel, and R. Wiesendanger, Nature (London U. K.) **447**, 190 (2007).
[15] G. Chen, T. P. Ma, A. T. N'Diaye, H. Y. Kwon, C. Won, Y. Z. Wu, and A. K. Schmid, Nat. Commun. **4**, 2671 (2013).
[16] S. Rohart and A. Thiaville, Phys. Rev. B **88**, 184422 (2013).
[17] A. Thiaville, S. Rohart, E. Jué, V. Cros, and A. Fert, Europhys. Lett. **100**, 57002 (2012).
[18] K. K. Meng, J. Miao, X. G. Xu, J. X. Xiao, J. H. Zhao, and Y. Jiang, Phys. Rev. B **93**, 060406(R) (2016).
[19] K. K. Meng, J. Miao, X. G. Xu, Y. Wu, X. P. Zhao, J. H. Zhao, and Y. Jiang, Phys. Rev. B **94**, 214413 (2016).
[20] M. Beg, R. Carey, W. Wang, D. Cortés-Ortuño, M. Vousden, M.-A. Bisotti, M. Albert, D. Chernyshenko, O. Hovorka, R. L. Stamps, and H. Fangohr, Sci. Rep. **5**, 17137 (2015).
[21] See Supplemental Material at http://link.aps.org/supplemental/10.1103/PhysRevB.97.060407 for details on additional analysis.
[22] D. Xiao, M.-C. Chang, and Q. Niu, Rev. Mod. Phys. **82**, 1959 (2010).
[23] L. A. Clevenger, A. Mutscheller, J. M. E. Harper, C. Cabral, Jr., and K. Barmak, J. Appl. Phys. **72**, 4918 (1992).
[24] L. Liu, C.-F. Pai, Y. Li, H. W. Tseng, D. C. Ralph, and R. A. Buhrman, Science **336**, 555 (2012).
[25] S. Woo, M. Mann, A. J. Tan, L. Caretta, and G. S. D. Beach, Appl. Phys. Lett. **105**, 212404 (2014).
[26] A. Sakuma, J. Magn. Magn. Mater. **187**, 105 (1998).
[27] A. Belabbes, G. Bihlmayer, F. Bechstedt, S. Blügel, and A. Manchon, Phys. Rev. Lett. **117**, 247202 (2016).
[28] W. Jiang, P. Upadhyaya, W. Zhang, G. Yu, M. B. Jungfleisch, F. Y. Fradin, J. E. Pearson, Y. Tserkovnyak, K. L. Wang,

O. Heinonen, S. G. E. te Velthuis, and A. Hoffmann, Science **349**, 283 (2015).

[29] F. Hellman, A. Hoffmann, Y. Tserkovnyak, G. Beach, E. Fullerton, C. Leighton, A. MacDonald, D. Ralph, D. Arena, H. Durr, P. Fischer, J. Grollier, J. Heremans, T. Jungwirth, A. Kimmel, B. Koopmans, I. Krivorotov, S. May, A. Petford-Long, J. Rondinelli *et al.*, Rev. Mod. Phys. **89**, 025006 (2017).

[30] L. J. Zhu, G. Woltersdorf, and J. H. Zhao, Sci. Rep. **6**, 34549 (2016).

[31] E. C. Stoner, Proc. R. Soc. London, Ser. A **165**, 372 (1938).